

# Pressure-Dependent Behavior of Defect-Modulated Band Structure in Boron Arsenide

Xianghai Meng, Akash Singh, Rinkle Juneja, Yanyao Zhang, Fei Tian, Zhifeng Ren, Abhishek K. Singh, Li Shi, Jung-Fu Lin,\* and Yaguo Wang\*

The recent observation of unusually high thermal conductivity exceeding  $1000 \text{ W m}^{-1} \text{ K}^{-1}$  in single-crystal boron arsenide (BAs) has led to interest in the potential application of this semiconductor for thermal management. Although both the electron/hole high mobilities have been calculated for BAs, there is a lack of experimental investigation of its electronic properties. Here, a photoluminescence (PL) measurement of single-crystal BAs at different temperatures and pressures is reported. The measurements reveal an indirect bandgap and two donor–acceptor pair (DAP) recombination transitions. Based on first-principles calculations and time-of-flight secondary-ion mass spectrometry results, the two DAP transitions are confirmed to originate from Si and C impurities occupying shallow energy levels in the bandgap. High-pressure PL spectra show that the donor level with respect to the conduction band minimum shrinks with increasing pressure, which affects the release of free carriers from defect states. These findings suggest the possibility of strain engineering of the transport properties of BAs for application in electronic devices.

Heat management has been a critical issue in ultralarge-scale integration technology as more and more transistors are confined onto a limited area when pursuing Moore's law. On the

Dr. X. Meng, Prof. L. Shi, Prof. Y. Wang  
Department of Mechanical Engineering  
The University of Texas at Austin  
Austin, TX 78712, USA  
E-mail: yaguo.wang@austin.utexas.edu

Dr. A. Singh, Dr. R. Juneja  
Materials Research Centre  
Indian Institute of Science  
Bangalore 560012, India

Y. Zhang, Prof. A. K. Singh, Prof. J.-F. Lin  
Department of Geological Sciences  
Jackson School of Geosciences  
The University of Texas at Austin  
Austin, TX 78712, USA  
E-mail: afu@jsg.utexas.edu

Dr. F. Tian, Prof. Z. Ren  
Department of Physics and Texas Center for Superconductivity  
at the University of Houston (TcSUH)  
University of Houston  
Houston, TX 77204, USA

Prof. L. Shi, Prof. J.-F. Lin, Prof. Y. Wang  
Texas Materials Institute  
The University of Texas at Austin  
Austin, TX 78712, USA

 The ORCID identification number(s) for the author(s) of this article can be found under <https://doi.org/10.1002/adma.202001942>.

DOI: 10.1002/adma.202001942

way to achieve high device density, heat dissipation is becoming more critical.<sup>[1]</sup> In order to dissipate heat more effectively, researchers have been investigating alternative materials with high thermal conductivity. Among all the materials, diamond possesses the highest thermal conductivity. The advent of polycrystalline chemical vapor deposition (CVD) diamond makes wafer-scale coverage possible with wide range of thermal grades, offering flexible applications in heat management,<sup>[2]</sup> such as GaN-on-diamond radio frequency transistors<sup>[3]</sup> and AlGaIn/GaN high-electron-mobility transistors on free-standing CVD diamond substrates.<sup>[4]</sup> However, the practical application of CVD diamond still suffers from slow growth rate, high cost, challenges in integration with semiconductors.<sup>[5,6]</sup> Graphite, as another type of carbon-based material,

even though could also offer high thermal conductivity, only along the in-plane direction. Moreover, the electronic band structures of diamond (insulators) and graphite (semimetal), restrain them from broader applications in electronics.<sup>[7]</sup>

Recently a new III–V compound boron arsenide (BAs) synthesized by chemical vapor transport (CVT) has been proven to have unusually high thermal conductivity.<sup>[6–8]</sup> BAs possesses the cubic zinc-blende structure with lattice constant = 0.4777 nm. The involvement of a heavy and a light atom creates a large frequency gap between acoustic phonons and optical phonons, limiting the scattering, and leading to a high thermal conductivity. Except for the promising feature for heat management, the semiconducting nature of BAs also gives potential as novel electronic materials, since BAs is predicted to simultaneously have high electron/hole mobility.<sup>[9]</sup> Unlike the insulating diamond or the semi-metallic graphene, BAs has a direct bandgap of  $\approx 4.1 \text{ eV}$ ,<sup>[10]</sup> and an indirect bandgap lies close to 1.77–2.02 eV.<sup>[11–13]</sup> However, under current synthesis technique, many types of defects exist in BAs crystal, such as C, Si, O, etc.<sup>[13,14]</sup> The non-uniform distribution of defects induces a large variation of measured thermal conductivity values, even in the same single crystal. Free carriers contributed by defects could scatter phonons and suppress thermal conductivity significantly,<sup>[8,13,15]</sup> but the effects of defects on the electronic band structure of BAs are largely unknown and require further investigation. The defect-modulated electronic band structure could be further altered by extrinsic approaches. Hydrostatic pressure generated in a diamond anvil cell (DAC) is an effective

tool to apply strain and tune physical properties in a large variety of materials. Representative examples are superconductivity in superhydride,<sup>[16]</sup> semiconductor-to-metal transition in transition metal dichalcogenides (TMDs),<sup>[17]</sup> and phase transition of GaTe.<sup>[18]</sup> One particular example is the strain-induced thermal conductivity enhancement by  $\approx 7X$  observed in MoS<sub>2</sub> at 15 GPa.<sup>[19]</sup> Hence, investigating the strain/pressure-dependent electronic band structure and impurities levels of BAs could enable new functionalities for electronic devices.

In this study, we investigated the temperature-/pressure-dependent behavior of defect-modulated electronic band structure in BAs single crystals using photoluminescence (PL) and Raman spectroscopy in a cryostat or a DAC as well as first-principles calculations. With the low-temperature PL and first-principles calculations, the intrinsic indirect bandgap and defect-related energy states were identified, where donor-acceptor pair (DAP) recombination were found to play a significant role, suppressing the indirect bandgap transition at ambient temperature. Under pressure, our Raman spectra display phonon hardening effect and a longitudinal optical/transverse optical (LO-TO) phonon splitting. The pressure-dependent PL spectra show that both the indirect bandgap and DAP recombination peaks redshift with pressure. Based on first-principles calculation results, the shift is attributed to a combined effect of the bandgap shrinkage and ionization energy reduction. Our studies reveal the defect-modulated electronic band structure in BAs crystal and the tunability of its electronic band structure with pressure, which shine light on their potential as high-power electronic materials.

We first perform Raman spectroscopy on BAs single crystal to characterize the pressure-dependent crystal structure and vibrational properties, as shown in **Figure 1**. The BAs crystal is loaded into a DAC with 500  $\mu\text{m}$  culet size, as shown in the inset of Figure 1b. Neon (Ne) is utilized as the pressure medium to maintain the hydrostatic pressure condition. A ruby sphere, which is used to calibrate the pressure, is placed on the culet as well, but not too close to the crystal, to avoid the interference between the later PL measurements ( $\approx 1.4\text{--}1.8$  eV) and the ruby fluorescence ( $\approx 1.78$  eV). R1 peak of ruby fluorescence is used to monitor the pressure inside the DAC. We perform

measurement from ambient pressure up to  $\approx 20$  GPa with increment  $\approx 1\text{--}2$  GPa.

Pressure-dependent Raman spectra are plotted in Figure 1a. At ambient pressure, the Raman spectrum shows two peaks at 697.7 and 720.8  $\text{cm}^{-1}$ , corresponding to the vibrational modes from <sup>11</sup>B and <sup>10</sup>B isotopes,<sup>[6,20]</sup> respectively. The difference between <sup>11</sup>B and <sup>10</sup>B peaks is 23.1  $\text{cm}^{-1}$ . This feature is peculiar and unique in BAs, because the previously reported Raman peaks of <sup>11</sup>B and <sup>10</sup>B in other compounds only show Raman peaks from the random mixing of both isotopes.<sup>[21]</sup> With increasing pressure, both the <sup>11</sup>B and <sup>10</sup>B peaks blueshift due to phonon hardening. Figure 1b plots the fitted Raman peak shifts as a function of pressure. The <sup>10</sup>B Raman peak shifts at a rate of 6.36  $\text{cm}^{-1}$  GPa<sup>-1</sup>, faster than that of <sup>11</sup>B peak at a rate of 4.34  $\text{cm}^{-1}$  GPa<sup>-1</sup>. At 19.4 GPa, the difference between the <sup>11</sup>B and <sup>10</sup>B peaks is about 39.1  $\text{cm}^{-1}$ , 16  $\text{cm}^{-1}$  larger than that at ambient condition. One interesting feature is that the <sup>11</sup>B Raman peak splits into two peaks starting from  $\approx 4$  GPa and this split increases with pressure, eventually reaches 7.1  $\text{cm}^{-1}$  at 19.4 GPa. This phenomenon, according to the first-principles calculations by Ravi-chandran et al., comes from the LO/TO phonon splitting,<sup>[22]</sup> as a result of different hardening rates between the LO and TO phonons at high pressure. According to the calculations, LO/TO splitting already exists at ambient condition. However, the splitting is only detectable experimentally at elevated pressures due to the limited resolution of our Raman system. The increasing trend of LO-TO phonon splitting in BAs with pressure is unusual comparing with other zinc-blende semiconductors, which is a result of more negative Born effective charge with pressure (polarization between B and As increases), as suggested by DFT calculations (Table S1 in Section S4, Supporting Information). We did not observe any splitting of the <sup>10</sup>B peak, possibly due to the much lower <sup>10</sup>B concentration (<sup>11</sup>B/<sup>10</sup>B 4:1) and very weak <sup>10</sup>B Raman peak. Previous studies showed that BAs undergoes zinc-blende (ZB) to rock-salt phase transition at pressures around 93 to 141 GPa.<sup>[23-27]</sup> A recent study also proposed some possible low-pressure phases (6H structure at 14.7 GPa, 10H-ZnS structure at 9.7 GPa),<sup>[28]</sup> however, we did not observe any features in our pressure-dependent Raman spectra indicating the formation of the new phase. So the BAs crystals

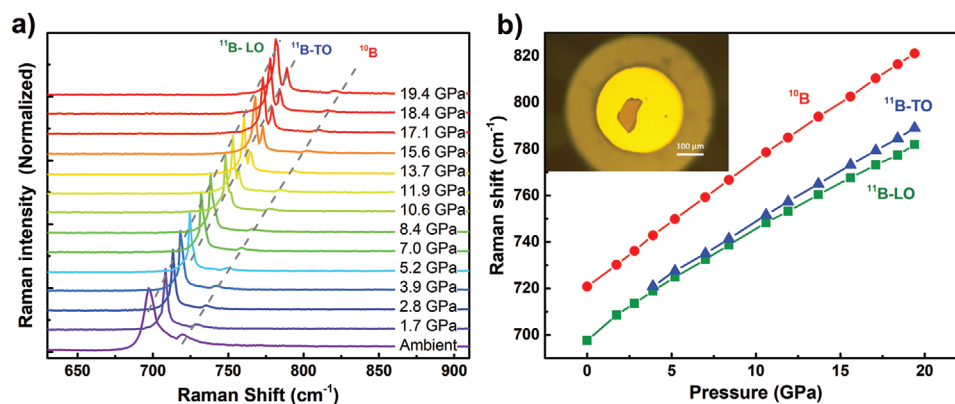


**Figure 1.** Experimental data and fitting result of Raman spectra at high pressure. a) Raman spectra of BAs from ambient pressure to 20 GPa (dashed lines are guide to the eye). b) Pressure-dependent Raman shifts for B-TO and B-LO modes at high pressure. Effects of boron isotopes, <sup>10</sup>B and <sup>11</sup>B from sample growth, can be seen clearly in Raman shifts. Image inset is the optical image of BAs sample loaded in a DAC.

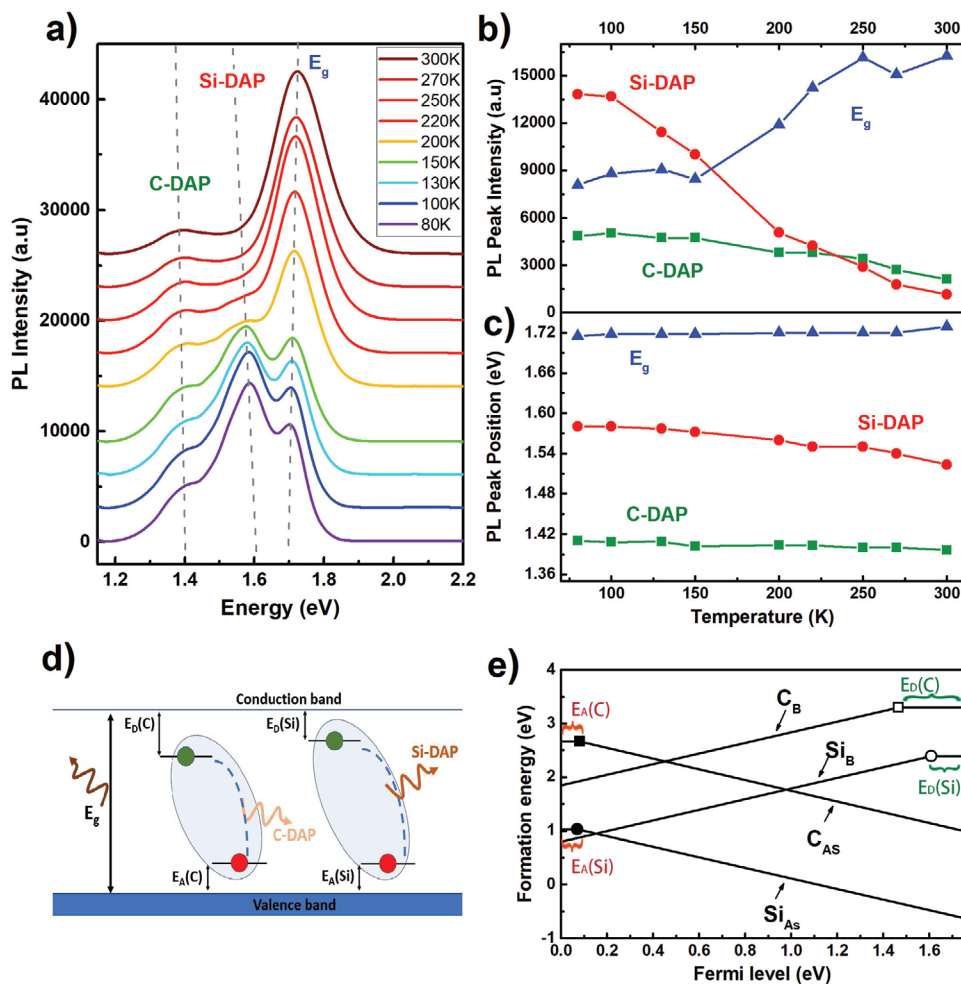


**Figure 2.** Experimental data and fitting result of PL spectra at low temperatures. a) Experimental data of PL of BAs crystal from 80 to 300 K. b) Fitted PL peak intensity versus temperature. c) Fitted PL peak shift versus temperature. d) Schematic of DAP recombination process, illustrating three optical transitions, which are from indirect bandgap, C-DAP recombination, and Si-DAP recombination, respectively. e) First-principles calculations on the formation energy versus Fermi level (from VBM), showing DAP recombination of C and Si defects in BAs. Open symbols correspond to donor levels of impurities, solid symbols correspond to acceptor levels of impurities. The squares and circles represent Si and C impurity levels, respectively (CB and SiB represent C/Si occupying B sites, which are donor levels releasing free electrons; CAs and SiAs represent C/Si occupying As sites, which are acceptor levels releasing free holes).

remain in the single ZB phase throughout the pressure range in our measurement.

With current synthesis technology, impurities exist in the BAs crystals,<sup>[13]</sup> which affect their electronic and thermal behaviors. With PL spectroscopy, we study the effect of impurities on the electronic band structure of BAs crystal. Low-temperature PL has been widely employed to reveal the details of electronic band structures. To cool down the BAs crystal, our sample is placed on a Si substrate, which is glued to the Cu sample holder with thermal conduction paste. The Cu holder is loaded inside a Janis ST-500 microscopy cryostat with liquid nitrogen as the cooling agent. The temperature is monitored by a built-in Si diode sensor through its voltage–temperature correlation. **Figure 2a** summarizes the PL spectra of BAs at temperatures ranging from 80 K to 300 K. Details of the raw PL spectra and signal processing can be found in Figure S1, Supporting Information. At ambient temperature, the spectra show two

dominant peaks, located at about 1.4 (left) and 1.73 eV (right), where the 1.73 eV peak has much higher intensity than the 1.4 eV one. When the temperature decreases, a third peak ( $\approx 1.6$  eV at 80 K) starts to appear and grows rapidly, eventually becomes dominating at 80 K.

We then perform Gaussian fitting to all the PL spectra. Examples of fitted results can be found in Figure S2, Supporting Information. Plotted in Figure 2b,c are the temperature-dependent intensities and peak positions of the three PL peaks. We find that the 1.4 eV peak and the 1.6 eV peak have similar temperature-dependent feature, where their intensities increase when temperature decreases; while the 1.73 eV peak has an opposite trend. We tentatively assume the 1.4 eV and the 1.6 eV peaks share the same origin, which is different from that of the 1.73 eV peak. To understand the nature of these PL peaks, we perform first-principles calculations to calculate the electronic band structure of BAs using HSE06 hybrid functional. Details

of the calculation methods can be found in Section S2, Supporting Information. As shown in Figure 4a, the direct bandgap of BAs occurs at  $\Gamma$ - $\Gamma$ , with a transition energy of 4.1 eV, which exceeds the range of our PL spectrometer. However, BAs also possesses an indirect bandgap, which occurs between valence band maximum (VBM) at  $\Gamma$  point and conduction band minimum (CBM) close to X point. DFT calculations predict this indirect transition to be 1.75 eV. This value agrees with the 1.71 eV (80 K, 1.73 eV at 300 K) PL peak in our measurement, as shown in Figure 2c. We assign the 1.71 eV PL peak to the indirect optical bandgap of BAs. Compared to other literatures of the first-principles calculations on the band structure of BAs (Table S2, Supporting Information), our calculated indirect bandgap is slightly larger than those predicted using local density approximation (LDA),<sup>[29,30]</sup> but comparable with or smaller than the values predicted with GW method.<sup>[10,11]</sup> LDA is known to underestimate the bandgap,<sup>[31,32]</sup> and the quasiparticle bandgap predicted with GW method is usually much higher than the optical bandgap. Even though HSE06 also predicts a quasiparticle bandgap, it is the most popular approach to simulate the optical and thermodynamic transitions associated with defect levels.<sup>[31,33–35]</sup> Our simulated value of 1.75 eV is consistent with the results in the literature using HSE06 (1.6–1.9 eV).<sup>[36–38]</sup> Moreover, our calculations did not consider spin orbit interaction, which may shift the bandgap by  $\approx 100$  meV.

Next step is to determine the nature of the 1.4 eV and 1.6 eV peaks. As shown in Figure 2b, the PL intensities of both 1.4 eV and 1.6 eV peaks decrease monotonically with increasing temperature, which is a typical feature of DAP recombination process caused by the thermal quenching of PL emission at high temperatures.<sup>[39,40]</sup> As shown in Figure 2d, upon optical excitation, electrons and holes are trapped at donor and acceptor levels to form neutral DAP excitons, which can luminesce efficiently. BAs is known to have a p-type conductivity,<sup>[13,41]</sup> which originates from free holes released from acceptor levels. The native defects, such as B or As vacancies, can only generate deep levels in the bandgap (close to the middle), which are difficult to be ionized, thus are unlikely to account for the apparent p-type conducting behavior.<sup>[13]</sup> Foreign atoms introduced during the synthesis process usually generate shallow donor/acceptor levels.<sup>[42]</sup> Measurement with time-of-flight secondary-ion mass spectrometry (TOF-SIMS) reveals several types of foreign atoms in BAs crystals, including Si, C, O, S, and F. (Figure S3, Supporting Information). Among these defects, Si and C are abundant and both have four valence electrons in the outermost shell ( $3s^23p^2$  for Si and  $2s^22p^2$  for C), hence can serve as both donors and acceptors in BAs. From Figure 2e, the formation energy of C is higher than Si, and the concentration of  $C_B$  is estimated to be around  $1.53 \times 10^{14} \text{ cm}^{-3}$ , and of  $C_{As}$  is around  $6.36 \times 10^{10} \text{ cm}^{-3}$ , with graphite as reference. In the literature, usually the concentration of DAP defects that induces photoluminescence falls into the range of  $10^{15}$  to  $10^{18} \text{ cm}^{-3}$ ,<sup>[43–45]</sup> higher than our simulated concentrations. However, with C defects in other initial form other than graphite, the formation energy will be lower, resulting in much higher concentration of  $C_B$  and  $C_{As}$ . Also our simulated values are the extreme case when Fermi level is exactly at VBM. In reality,  $C_B/C_{As}$  ratio could be more balanced, because the Fermi level of lightly doped p-type semiconductor (like BAs) is not at, but above VBM (see details

in Section S7, Supporting Information). Here we assume the defect concentrations are constant when cooling the crystals from growth temperature to room temperature. Even though oxygen defects are also abundant, DFT calculations suggested that  $O_B$  is always stable as neutral charge state and  $O_{As}$  provides very deep donor and acceptor levels with high formation energy (Figure S4, Supporting Information). Hence it is unlikely for oxygen defects to form DAP. Figure 2e shows the calculated ionization energies of Si and C at different Fermi levels, where  $E_A(C) = 0.081$  eV (C replacing As as acceptors),  $E_D(C) = 0.283$  eV (C replacing B as donors),  $E_A(Si) = 0.07$  eV (Si replacing As as acceptors), and  $E_D(Si) = 0.14$  eV (Si replacing B as donors). The DAP recombination energy can be estimated as: C-DAP =  $E_g - E_A(C) - E_D(C) = 1.71$  (80K) - 0.081 - 0.283 = 1.35 eV; and Si-DAP =  $E_g - E_A(Si) - E_D(Si) = 1.71$  (80K) - 0.07 - 0.14 = 1.5 eV. These values agree with the measured peaks in PL spectra, C-DAP  $\approx 1.40$  eV at 80 K and Si-DAP  $\approx 1.58$  eV at 80 K. Therefore, we assign the 1.4 eV peak to C-DAP and the 1.6 eV peak to Si-DAP. Figure 2e also shows that the acceptor levels ( $C_{As}$  and  $Si_{As}$ ) usually have smaller formation energy than the donor levels ( $C_B$  and  $Si_B$ ), thus are more stable and contribute to the p-type conductivity of BAs.

Now we can analyze the temperature-dependent PL intensities and peak positions in Figure 2b,c. The PL intensity of  $E_g$  peak increases dramatically with temperature, while those of both the C-DAP and Si-DAP peaks show substantial decrease. These opposite trends could be attributed to the temperature-dependent thermal activation energy. At low temperature, when thermal energy is not enough to ionize the DAP excitons, these bound excitons have a high probability to recombine at the DAP levels, leading to high intensity of the DAP peaks. As the temperature increases to some point ( $\approx 150$  K as seen in Figure 2b), thermal energy would be sufficient to disassociate the DAP bound exciton and cause them to return to the free exciton level. These free excitons would recombine at the energy of indirect bandgap, resulting in a higher intensity of  $E_g$  peak. The overall effect is, with increasing temperature, the free exciton intensity increase at the expense of bound excitons intensity.<sup>[46]</sup> Above 250 K, the intensity of  $E_g$  saturates and those of C-DAP and Si-DAP peaks become very small, which indicates that most DAP excitons are thermally activated. The PL peak positions of C-DAP and Si-DAP show slight redshifts with temperature, which is a common behavior considering the weakened interatomic bond and shallower potential seen by the electrons in the material.  $E_g$  peak has almost negligible dependence on temperature. When lowering the temperature, the slight increasing trend in bandgap from the shrinkage of interatomic spacing would be offset by the weakened free-carrier screening effect, thus the bandgap variation with temperature is small. (See Section S6, Supporting Information.)

Plotted in Figure 3a are the pressure-dependent PL spectra. All the three PL peaks,  $E_g$ , C-DAP, and Si-DAP, display redshift with pressure. Figure 3b,c shows the fitted pressure-dependent peak positions and widths. The indirect bandgap shrinks from 1.73 eV to 1.62 eV when pressure increases from 0 GPa to 19.4 GPa, at a rate of  $\approx 5.15 \text{ meV GPa}^{-1}$ , which is consistent with previous theoretical calculations ( $4.7 \text{ meV GPa}^{-1}$ ).<sup>[26]</sup> Si-DAP peak also has a redshift of about 0.1 eV with a same rate of  $\approx 5.15 \text{ meV GPa}^{-1}$ . Pressure tuning effect on C-DAP is much

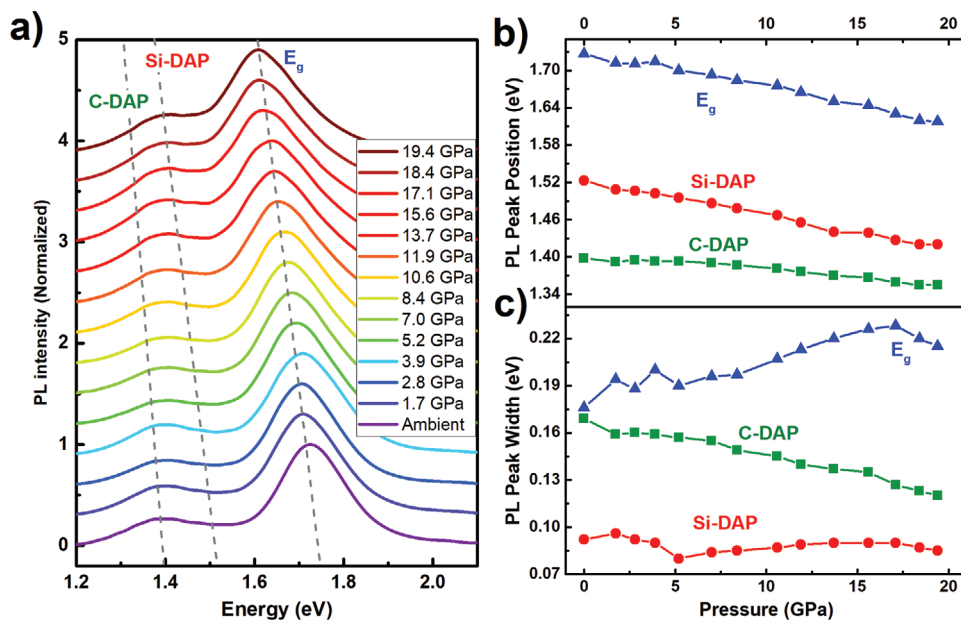


**Figure 3.** Experimental data and fitting result of PL spectra at high pressure. a) Experimental data of PL spectra from ambient pressure to 20 GPa. b) Fitted PL peak position versus pressure. c) Fitted PL peak width versus pressure.

weaker, about 0.04 eV redshift at a rate of  $\approx 2.06$  meV  $\text{GPa}^{-1}$ . Pressure tuning on the BAs band structure and the donor/acceptor levels of C and Si impurities are also computed with first-principles calculations. Figure 4a,b compares the band structure at ambient condition and 20.6 GPa, respectively. The band structure change at intermediate pressures was also calculated and presented in Figure S8, Supporting Information (Section S9, Supporting Information). At ambient pressure, the position of VBM occurs at the  $\Gamma$  point, while the CBM occurs along the  $\Gamma$  to X direction at a k-point with crystal coordinates (0.39, 0.00, 0.39), about 80% of the distance to the X point. With pressure, the position of VBM shifts upward, while the position of CBM shifts downward. The indirect bandgap is reduced by 12%, from 1.75 eV at 0 GPa to 1.54 eV at 20 GPa, consistent to the trend observed in our experiment (Figure 3b). On the contrary, the direct bandgap and transitions at high-symmetry points, such as L-L, K-K, X-X, all increase with pressure. Simulation results (Figure S9, Supporting Information) also suggest that both tensile and compressive strain uplifts the VBM and downshifts the CBM. With 3.8% compressive strain, the indirect bandgap decreases from 1.75 eV to 1.54 eV; with 3.8% compressive strain, the indirect bandgap decreases from 1.75 eV to 1.48 eV. The resulted deformation potential at VBM is nearly 0.02 eV and at CBM is about 0.03 eV.

Plotted in Figure 4c are the pressure-dependent acceptor/donor levels with respect to VBM and CBM (marked as dashed lines). CBM decreases with pressure (orange arrow). The acceptor levels of  $C_{As}$  and  $Si_{As}$  (solid symbols) with respect to the VBM are almost constant ( $\approx 0.08$  eV, in light blue shade) at different pressures. In contrast, the donor levels of  $C_B$  and  $Si_B$  (open symbols, in yellow shade) become shallower with pressure. The difference between donor levels and CBM, represented by the length of the solid line between open symbol and a dashed vertical line, is the ionization energy of carriers

on specific donor level,  $E_D$ . For both  $C_B$  and  $Si_B$ , the ionization energy becomes smaller at high pressure. For  $C_B$ , the ionization energy ( $E_D$ ) are 0.28 (0 GPa), 0.3 (4.5 GPa), 0.28 (8.8 GPa), 0.2 (14.3 GPa) and 0.16 eV (20 GPa); for  $Si_B$ , the  $E_D$  are 0.21 (0 GPa), 0.19 (4.5 GPa), 0.12 (8.8 GPa), 0.1 (14.3 GPa) and 0.055 eV (20 GPa). The DAP recombination energy, represented by the horizontal distance between open and solid symbols, decreases with pressure. These calculated results agree with experiments (Figure 3b), and the decreasing PL positions with increasing pressure come from a combined effect of both indirect-bandgap shrinkage and donor level ionization energy decrease at high pressure.

The decrease in donor level ionization energy will have another impact on the measured PL spectra. As shown in Figure 3c, the peak width (FWHM) of  $E_g$  becomes broader with pressure, from 0.176 to 0.215 eV. This phenomenon has been routinely observed in high-pressure PL and Raman measurements.<sup>[47,48]</sup> The strengthened crystal field at high pressure can induce larger band splitting and enhance electro-phonon coupling at high pressure.<sup>[49]</sup> Conversely, the two DAP PL peaks become narrower at high pressure, which is counterintuitive. This feature is unique in BAs and has not been reported in other material systems. PL peak width is usually taken as an indicator of carrier lifetime. The narrower width at high pressures means longer lifetime for carriers on donor/acceptor levels. As mentioned earlier, BAs shows p-type conductivity wherein holes are the majority carriers and electrons are minority carriers. When the excited carrier concentration is small compared to the majority carriers, PL decay time corresponds to minority carrier lifetime.<sup>[50]</sup> The pressure-dependent PL width in Figure 3c illustrates that the lifetime of minority carriers in BAs (electrons) increase with pressure. This lifetime elongation could be explained by the donor ionization energy ( $E_D$ ) reduction at high pressure, as shown in Figure 4d.

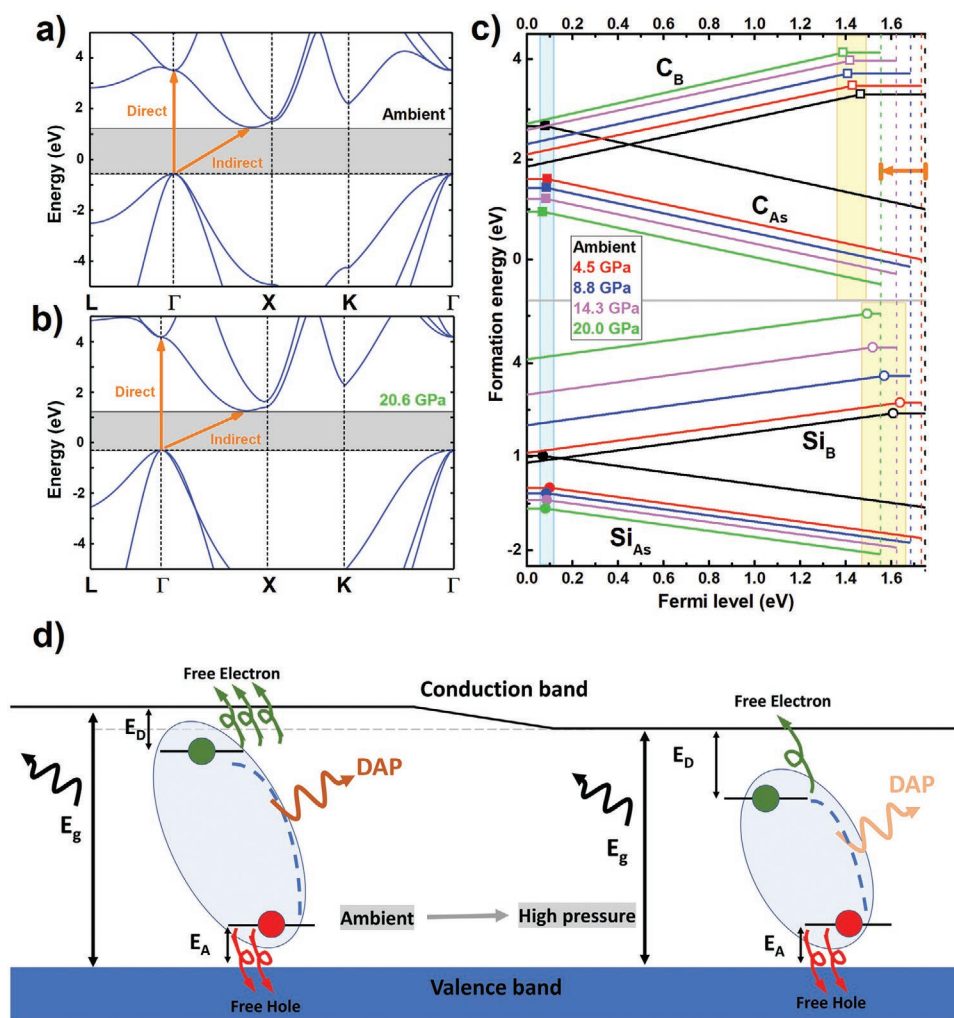


**Figure 4.** First-principles calculations of the band structure and formation energy of impurities. a,b) First-principles calculations of BAs band structures at ambient pressure and 20.6 GPa. c) Pressure dependent donor/acceptor levels of C (upper panel) and Si (lower panel) in BAs. Open symbols are for donor levels of impurities, solid symbols are acceptor levels of impurities. The squares represent Si impurities levels, and the circles represent C impurity levels. The lines and symbols with different colors represent different pressures. The vertical dashed lines on the very right correspond to the CBM at different pressures. The orange arrow indicates the decrease of the indirect bandgap with increasing pressure. The regions shaded with light blue and light yellow highlight the donor/acceptor level change with pressure, where acceptor levels of both CAs and SiAs are insensitive to pressure, and donor levels of CAs and SiAs decrease with pressure. d) Schematics picture of the pressure effect on the PL photon energy and the free carriers release. The energy levels changes are exaggerated for illustration purposes.

Ionization energy is proportional to carrier effective mass, which becomes smaller at higher pressure.<sup>[51]</sup> Because of the smaller ionization energy with respect to the CBM, electrons from the donor levels can be ionized more easily to become free carriers. These free carriers can either recombine at the  $E_g$  level or be recaptured by the donor levels and still recombine at the donor levels. The latter process would give a longer effective lifetime of DAP recombination, as shown in Figure 3c. This phenomenon is expected to be more prominent when  $E_D$  approaches the thermal energy activation (0.026 eV at room temperature). In our range of applied pressure, the  $E_D$  values are still larger than 0.026 eV, which explains the moderate decrease of FWHM for both Si-DAP and C-DAP.

In summary, we carried out both Raman and PL measurement on CVT-grown BAs single crystals and studied their

temperature-/pressure-dependent behavior of the electronic band structure. We observed the Raman peaks of two isotopes (<sup>11</sup>B and <sup>10</sup>B). The splitting of <sup>11</sup>B LO/TO phonons becomes more prominent at high pressure, which is a result of more negative Born effective charge ( $Z^*$ ) with pressure, as suggested by DFT calculations. Increase of  $Z^*$  means the polarization between cations (As) and anions (B) increases, which causes the increase of splitting between LO–TO phonons. Negative Born effective charge of boron also indicates a reverse role of anions and cations in BAs (boron as anion), in contrast to that expected from normal oxidation states like GaAs. The reason for this unexpected phenomenon is the anomalously low energy of the boron p orbitals and strong s–s repulsion, indicating a high degree of covalency in the bonding between B and As.

Temperature-dependent PL spectra reveal three dominant transitions, at indirect bandgap of  $\approx 1.73$  eV and at two pairs of donor/acceptor levels introduced by C and Si impurities. PL measurements at high pressure show that all the three transitions are highly tunable under strain, which comes from a combined effect of indirect-bandgap shrinkage and ionization energy reduction at donor level. On the contrary, simulations suggest that the direct bandgap and transitions at high-symmetry points, such as L–L, K–K, X–X, all increase with pressure (Figure S8, Supporting Information). These results confirm the existence of optical transitions lower than the intrinsic indirect bandgap. This finding could explain the smaller values of previously reported bandgaps measured with different techniques, such as optical transmission,<sup>[52]</sup> optical absorption,<sup>[53]</sup> photo-to-electron conversion efficiency,<sup>[41]</sup> etc., where the impurity levels might be probed instead.

The major mechanism of defects interaction with carriers are recombination at DAP levels formed by C and Si impurities. Defect-carrier interaction determines the carrier transport properties, such as mobility. The ionization energies of these DAP levels are highly tunable with temperature and pressure. With simulation the effect of strain on the band edges (Figure S10, Supporting Information) was also analyzed. The calculated deformation potential is small comparing with that of Si,<sup>[54]</sup> GaAs,<sup>[55]</sup> and ZnO<sup>[56]</sup> and suggests a high mobility. Combining all these factors: high carrier mobility, wide energy bandgaps, and high thermal conductivity of BAs, BAs is a promising material for future advanced electronic and optoelectronic applications.

Recently, 2D h-BAs has been predicted by first-principles calculations with structure similar to graphene and TMDs.<sup>[57,58]</sup> Intrinsically h-BAs would be a direct bandgap semiconductor with a bandgap  $\approx 1$  eV, and this semiconducting nature could be preserved up to 7% strain. Furthermore, the in-plane thermal conductivity could be enhanced by 2 $\times$  with only 3% tensile strain. These unique features make h-BAs a potentially desirable material for future thermal management in electronic devices. However, further experimental investigations are required to validate these theoretical predictions.

## Experimental Section

**Sample Information:** BAs single crystals were grown in a sealed quartz tube through CVT method. Pure boron bulk particles, arsenic lumps, and iodine powder were positioned at one end of a sealed quartz tube, and as-grown BAs tiny single crystals or other materials were carefully placed on the other end of the tube to serve as seeds. A temperature gradient was maintained between the seeds side and the source side for 14 days. The BAs crystals appear at the seed zone were then cleaned by aqua regia to remove the residues for DAC measurements. Details of the growth process can be found in previous reports.<sup>[7]</sup> For high-pressure measurement, the sample is cut by a sharp-edge knife to be  $\approx 150 \mu\text{m} \times 75 \mu\text{m}$  to fit inside the DAC. Also the sample is double-side polished so that the top and bottom surfaces both sit flat on the diamond surface.

**High-Pressure Photoluminescence and Raman Measurement:** Our DAC has 500  $\mu\text{m}$  culet size, with a gasket drilling hole about 320  $\mu\text{m}$  in diameter. The pressure medium we used is Neon. Both PL and Raman spectra were taken with Renishaw In-via Raman system with 532 nm laser excitation. The laser beam was focused to a 5  $\mu\text{m}$  spot ( $1/e^2$  diameter) onto sample surface with a 20 $\times$  long-working-distance objective lens. Signals are collected through the same objective lens and

sent to diffraction grating and charge-coupled device for data acquisition. Raman and PL measurements were carried out with 2400  $\text{mm}^{-1}$  and 1200  $\text{mm}^{-1}$  gratings, respectively.

In high-pressure measurement, pressure is calibrated with the fluorescence of the R1 peak of the ruby sphere by the following equation:<sup>[59,60]</sup>

$$P = \frac{A}{B} \left\{ \left[ 1 + \frac{\Delta\lambda}{\lambda_0} \right]^B - 1 \right\} \quad (1)$$

Every time after the pressure was adjusted, data was recorded after certain time so that the pressure was stabilized. Since our measurement running time is short (<15 min), the pressure change during the each measurement could be neglected. The uncertainty of the pressures at different locations in the DAC could be estimated to be smaller than 0.15 GPa at 20 GPa from previous publications. So, the total uncertainty of the pressure should be less than 0.15 GPa until 20 GPa.

## Supporting Information

Supporting Information is available from the Wiley Online Library or from the author.

## Acknowledgements

X.M. and A.S. contributed equally to this work. The authors are grateful for the support from National Science Foundation (NASCENT, Grant No. EEC-1160494; CAREER, Grant No. CBET-1351881, CBET-1707080, Center for Dynamics and Control of Materials DMR-1720595); A.K.S., R.J., and A.S. thank the Materials Research Centre and Supercomputer Education and Research Centre of Indian Institute of Science for providing computing facilities. A.K.S., R.J., and A.S. acknowledge the support from Institute of Eminence (IoE) MHRD grant of Indian Institute of Science. F.T., L.S., and Z.F.R. were supported by Office of Naval Research (ONR) MURI grant N00014-16-1-2436. The authors thank Dr. Andrei Dolocan at TMI of University of Texas at Austin for his help on the TOF-SIMS measurements.

## Conflict of Interest

The authors declare no conflict of interest.

## Keywords

band structure, boron arsenide, high pressure, impurities, photoluminescence

Received: March 20, 2020

Revised: September 2, 2020

Published online:

- [1] J. Kim, D. A. Evans, D. P. Sellan, O. M. Williams, E. Ou, A. H. Cowley, L. Shi, *Appl. Phys. Lett.* **2016**, *108*, 201905.
- [2] R. Balmer, J. Brandon, S. Clewes, H. Dhillon, J. Dodson, I. Friel, P. Inglis, T. Madgwick, M. Markham, T. Mollart, *J. Phys.: Condens. Matter* **2009**, *21*, 364221.
- [3] J. Pomeroy, M. Bernardoni, A. Sarua, A. Manoi, D. Dumka, D. Fanning, M. Kuball, presented at *2013 IEEE Compound Semiconductor Integrated Circuit Symposium (CSICS)*, Monterey, CA, USA **2013**.

- [4] K. D. Chabak, J. K. Gillespie, V. Miller, A. Crespo, J. Roussos, M. Trejo, D. E. Walker, G. D. Via, G. H. Jessen, J. Wasserbauer, *IEEE Electr. Device Lett.* **2009**, *31*, 99.
- [5] L. Lindsay, D. Broido, T. Reinecke, *Phys. Rev. Lett.* **2013**, *111*, 025901.
- [6] J. S. Kang, M. Li, H. Wu, H. Nguyen, Y. Hu, *Science* **2018**, *361*, 575.
- [7] F. Tian, B. Song, X. Chen, N. K. Ravichandran, Y. Lv, K. Chen, S. Sullivan, J. Kim, Y. Zhou, T.-H. Liu, *Science* **2018**, *361*, 582.
- [8] S. Li, Q. Zheng, Y. Lv, X. Liu, X. Wang, P. Y. Huang, D. G. Cahill, B. Lv, *Science* **2018**, *361*, 579.
- [9] T.-H. Liu, B. Song, L. Meroueh, Z. Ding, Q. Song, J. Zhou, M. Li, G. Chen, *Phys. Rev. B* **2018**, *98*, 081203.
- [10] K. Bushick, K. Mengle, N. Sanders, E. Kioupakis, *Appl. Phys. Lett.* **2019**, *114*, 022101.
- [11] B. Song, K. Chen, K. Bushick, K. A. Mengle, F. Tian, G. A. G. U. Gamage, Z. Ren, E. Kioupakis, G. Chen, *Appl. Phys. Lett.* **2020**, *116*, 141903.
- [12] J. S. Kang, M. Li, H. Wu, H. Nguyen, Y. Hu, *Appl. Phys. Lett.* **2019**, *115*, 122103.
- [13] J. L. Lyons, J. B. Varley, E. R. Glaser, J. A. Freitas Jr, J. C. Culbertson, F. Tian, G. A. Gamage, H. Sun, H. Ziyadee, Z. Ren, *Appl. Phys. Lett.* **2018**, *113*, 251902.
- [14] J. Xing, E. R. Glaser, B. Song, J. C. Culbertson, J. A. Freitas Jr, R. A. Duncan, K. A. Nelson, G. Chen, N. Ni, *Appl. Phys. Lett.* **2018**, *112*, 241903.
- [15] J. Zou, D. Kotchetkov, A. Balandin, D. Florescu, F. H. Pollak, *J. Appl. Phys.* **2002**, *92*, 2534.
- [16] M. Somayazulu, M. Ahart, A. K. Mishra, Z. M. Geballe, M. Baldini, Y. Meng, V. V. Struzhkin, R. J. Hemley, *Phys. Rev. Lett.* **2019**, *122*, 027001.
- [17] A. P. Nayak, S. Bhattacharyya, J. Zhu, J. Liu, X. Wu, T. Pandey, C. Jin, A. K. Singh, D. Akinwande, J.-F. Lin, *Nat. Commun.* **2014**, *5*, 3731.
- [18] A. Pawbake, C. Bellin, L. Paulatto, K. Béneut, J. Biscaras, C. Narayana, D. J. Late, A. Shukla, *Phys. Rev. Lett.* **2019**, *122*, 145701.
- [19] X. Meng, T. Pandey, J. Jeong, S. Fu, J. Yang, K. Chen, A. Singh, F. He, X. Xu, J. Zhou, W.-P. Hsieh, A. K. Singh, J.-F. Lin, Y. Wang, *Phys. Rev. Lett.* **2019**, *122*, 155901.
- [20] V. Hadjiev, M. Iliev, B. Lv, Z. Ren, C. Chu, *Phys. Rev. B* **2014**, *89*, 024308.
- [21] H. Werheit, V. Filipov, K. Shirai, H. Dekura, N. Shitsevalova, U. Schwarz, M. Armbrüster, *J. Phys.: Condens. Matter* **2011**, *23*, 065403.
- [22] N. K. Ravichandran, D. Broido, *Nat. Commun.* **2019**, *10*, 827.
- [23] M. Sarwan, P. Bhardwaj, S. Singh, *Chem. Phys.* **2013**, *426*, 1.
- [24] L. Bing, L. Rong-Feng, Y. Yong, Y. Xiang-Dong, *Chin. Phys. B* **2010**, *19*, 076201.
- [25] M. Talati, P. K. Jha, *Int. J. Mod. Phys. B* **2010**, *24*, 1235.
- [26] A. Boudjemline, M. M. Islam, L. Louail, B. Diawara, *Physica B* **2011**, *406*, 4272.
- [27] R. M. Wentzcovitch, M. L. Cohen, P. K. Lam, *Phys. Rev. B* **1987**, *36*, 6058.
- [28] L. Wang, F. Tian, X. Liang, Y. Fu, X. Mu, J. Sun, X.-F. Zhou, K. Luo, Y. Zhang, Z. Zhao, *Phys. Rev. B* **2019**, *99*, 174104.
- [29] I. H. Nwigboji, Y. Malozovsky, L. Franklin, D. Bagayoko, *J. Appl. Phys.* **2016**, *120*, 145701.
- [30] L. L. Stevens, E. B. Orler, D. M. Dattelbaum, M. Ahart, R. J. Hemley, *J. Chem. Phys.* **2007**, *127*, 104906.
- [31] C. Freysoldt, B. Grabowski, T. Hickel, J. Neugebauer, G. Kresse, A. Janotti, C. G. Van de Walle, *Rev. Mod. Phys.* **2014**, *86*, 253.
- [32] P. Bogusławski, J. Bernholc, *Phys. Rev. B* **1997**, *56*, 9496.
- [33] A. Alkauskas, P. Broqvist, A. Pasquarello, *Phys. Rev. Lett.* **2008**, *101*, 046405.
- [34] A. Singh, A. K. Singh, *Phys. Rev. B* **2019**, *99*, 121201.
- [35] Y. Frodason, K. Johansen, T. Bjørheim, B. Svensson, A. Alkauskas, *Phys. Rev. B* **2017**, *95*, 094105.
- [36] Y. Ge, W. Wan, X. Guo, Y. Liu, *Opt. Express* **2020**, *28*, 238.
- [37] Q. Zheng, C. A. Polanco, M.-H. Du, L. R. Lindsay, M. Chi, J. Yan, B. C. Sales, *Phys. Rev. Lett.* **2018**, *121*, 105901.
- [38] S. Chae, K. Mengle, J. T. Heron, E. Kioupakis, *Appl. Phys. Lett.* **2018**, *113*, 212101.
- [39] A. Aydinli, N. Gasanly, I. Yilmaz, A. Serpengüzel, *Semicond. Sci. Technol.* **1999**, *14*, 599.
- [40] N. Gasanly, A. Serpengüzel, A. Aydinli, O. Gürlü, I. Yilmaz, *J. Appl. Phys.* **1999**, *85*, 3198.
- [41] S. Wang, S. F. Swingle, H. Ye, F.-R. F. Fan, A. H. Cowley, A. J. Bard, *J. Am. Chem. Soc.* **2012**, *134*, 11056.
- [42] R. Dingle, M. Ilegems, *Solid State Commun.* **1971**, *9*, 175.
- [43] A. Liu, H. T. Nguyen, D. Macdonald, *IEEE J. Photovoltaics* **2017**, *7*, 581.
- [44] D. Toginho Filho, I. Dias, J. Duarte, E. Laureto, J. C. Harmand, *Braz. J. Phys.* **2005**, *35*, 999.
- [45] M. Tajima, T. Iwai, H. Toyota, S. Binetti, D. Macdonald, *J. Appl. Phys.* **2011**, *110*, 043506.
- [46] A. K. Viswanath, J. I. Lee, S. Yu, D. Kim, Y. Choi, C.-h. Hong, *J. Appl. Phys.* **1998**, *84*, 3848.
- [47] A. P. Nayak, T. Pandey, D. Voiry, J. Liu, S. T. Moran, A. Sharma, C. Tan, C. Chen, L.-J. Li, M. U. Chhowalla, *Nano Lett.* **2015**, *15*, 346.
- [48] J. Barzowska, T. Lesniewski, S. Mahlik, H. J. Seo, M. Grinberg, *Opt. Mater.* **2018**, *84*, 99.
- [49] M. Runowski, P. Woźny, N. Stopikowska, Q. Guo, S. Lis, *ACS Appl. Mater. Interfaces* **2019**, *11*, 4131.
- [50] D. Donetsky, S. P. Svensson, L. E. Vorobjev, G. Belenky, *Appl. Phys. Lett.* **2009**, *95*, 212104.
- [51] V. Shchennikov, S. Ovsyannikov, *Solid State Commun.* **2002**, *121*, 323.
- [52] S. Ku, *J. Electrochem. Soc.* **1966**, *113*, 813.
- [53] T. Chu, A. Hyslop, *J. Electrochem. Soc.* **1974**, *121*, 412.
- [54] W. G. Vandenberghe, M. V. Fischetti, *Appl. Phys. Lett.* **2015**, *106*, 013505.
- [55] R. Mair, R. Prepost, E. Garwin, T. Maruyama, *Phys. Lett. A* **1998**, *239*, 277.
- [56] G. Callsen, J. S. Reparaz, M. R. Wagner, R. Kirste, C. Nenstiel, A. Hoffmann, M. R. Phillips, *Appl. Phys. Lett.* **2011**, *98*, 061906.
- [57] M. Raesi, S. Ahmadi, A. Rajabpour, *Nanoscale* **2019**, *11*, 21799.
- [58] M. R. Brems, M. Willatzen, *New J. Phys.* **2019**, *21*, 093030.
- [59] H. Mao, J.-A. Xu, P. Bell, *J. Geophys. Res.: Solid Earth* **1986**, *91*, 4673.
- [60] A. Dewaele, M. Torrent, P. Loubeyre, M. Mezouar, *Phys. Rev. B* **2008**, *78*, 104102.